THE ASTROPHYSICAL JOURNAL, 543:880–888, 2000 November 10

He 2-113: A MULTIPOLAR PLANETARY NEBULA WITH RINGS AROUND A COOL WOLF-RAYET STAR

RAGHVENDRA SAHAI,[1] LARS-ÅKE NYMAN,[2,3] AND ALWYN WOOTTEN[4]
Received 1999 December 9; accepted 2000 April 24

ABSTRACT

We present Hα imaging and molecular-line (CO) observations of He 2-113, an object which belongs to a rare class of planetary nebulae with Wolf-Rayet type central stars. The Hα images, obtained with the *Hubble Space Telescope* Wide-Field Planetary Camera 2, show that He 2-113 has an overall bipolar shape and two bright, knotty, compact ringlike structures around the central star. The major bipolar axis and the axis of symmetry of the rings are not colinear. A third, smaller, lobe is found to extend along an axis different from both of the above. The central star of He 2-113 is conspicuously offset from the geometrical centers of the rings and the main bipolar lobes. A faint extended round halo surrounds the bipolar nebula, probably representing the spherical mass-loss phase of the progenitor AGB red giant. The CO data indicate that this halo is mostly neutral and expanding at 28 km s^{-1}; an extended weak blue wing indicates that some of the molecular gas has been accelerated to significantly larger velocities. Self-consistent modeling of the CO data and *IRAS* far-infrared flux, including heating-cooling to calculate the gas kinetic temperature, shows that the mass-loss rate of the progenitor AGB star is relatively high ($\sim 10^{-4}\ M_\odot\ yr^{-1}$) and that the molecular gas is relatively cold; the gas-to-dust ratio (by mass) is 190. The very aspherical morphology of the He 2-113 nebula may allow ionizing radiation to escape preferentially from the nebula along directions with relatively low optical depth. The observed nebular structure is not consistent with the generalized interacting winds model of planetary nebula formation. The multilobed structure supports a new model by Sahai & Trauger in which collimated outflows with changing directionality are the primary agent for the shaping of planetary nebulae. The origin of the rings and the offset of the central star remain puzzling.

Subject headings: circumstellar matter — planetary nebulae: individual (He 2-113) — radio lines: ISM — stars: AGB and post-AGB — stars: mass loss

1. INTRODUCTION

Most planetary nebulae (PNe) show significant departures from spherical symmetry (e.g., Aaquist & Kwok 1991; Schwarz, Corradi, & Melnick 1992; Sahai & Trauger 1998, hereafter ST98), whereas the circumstellar envelopes (CSEs) of their progenitor AGB stars appear spherically symmetric (e.g., Bowers, Johnston, & Spencer 1983; Sahai & Bieging 1993; Neri et al. 1998). Why and how this happens is not understood and is a subject of great current interest. ST98 have proposed that collimated fast outflows with changing directionality, operating during the very late-AGB or the early post-AGB (hereafter proto–planetary phase), are the primary agents in the formation of aspherical PNe. Using the Wide Field and Planetary Camera 2 (WFPC2) onboard the *Hubble Space Telescope*[5] (*HST*), it has now become possible to image young planetary and proto–planetary nebulae (PPNe) with unprecedented angular resolution and dynamic range (Sahai 1999, 2000; Sahai et al. 1998, 1999a, 1999b, 1999c, 1999d; Kwok, Su, & Hrivnak 1998; Su et al. 1998). Such observations provide stringent constraints on the nature and history of mass loss during AGB and early post-AGB evolution, crucial for testing theories for the formation and shaping of PNe.

He 2-113 (also called PK 321+03 1, He 3-1044, IRAS 14562−5406) belongs to a small but important subclass of PNe (∼8%; Gorny & Stasinska 1995) which have WC Wolf-Rayet central stars (see Crowther, De Marco, & Barlow 1998 for a detailed description of the WC classification scheme). These stars, with strongly enhanced C and He but no observable H in their atmosphere, are the low-mass counterparts of population I Wolf-Rayet stars. The precise evolutionary status of these objects remains uncertain but may be related to a thermal pulse during the very early post-AGB phase, or very late when the central star is already on the white-dwarf cooling track (Iben et al. 1983).

Although detailed spectroscopic studies of He 2-113 have been carried out (le Bertre et al. 1989; De Marco, Barlow, & Storey 1997, hereafter DBS97; De Marco & Crowther 1998; Leuenhagen, Hamann, & Jeffrey 1996), the morphology of its nebula is poorly known. DBS97 deconvolved WFPC1 Hβ and [O III] λ5007 images of He 2-113, but found "very little structure." In this paper, we present and analyze high angular resolution optical imaging and millimeter-wave spectroscopic observations of He 2-113. These data allow us to probe the detailed structure of the compact nebula near the star, as well as the physical characteristics of the surrounding mass-loss envelope generated by the star near the end of its evolution on the AGB. Many of our quantitative results depend on the distance to He 2-113, which is uncertain (as is the case for most PNe). DBS97 made two estimates: (i) 1.5 ± 0.3 kpc, based on Magellanic cloud WR central star luminosities (revised by De Marco & Crowther 1998 to 1.23 kpc), and (ii) 1.9 kpc, based on the galactic rotation curve. We have conservatively adopted an intermediate value of 1.5 kpc in this paper.

[1] Jet Propulsion Laboratory, MS 183-900, California Institute of Technology, Pasadena, CA 91109; sahai@grandpa.jpl.nasa.gov.
[2] ESO/La Silla, Casilla 19001, Santiago 19, Chile.
[3] Onsala Space Observatory, S–439 92 Onsala, Sweden.
[4] NRAO, 520 Edgemont Road, Charlottesville, VA 22903-2475.
[5] the NASA/ESA *Hubble Space Telescope* is operated by the Space Telescope Science Institute (operated by AURA, Inc., under NASA contract NAS 5-26555).

The plan of our paper is as follows. In § 2, we give brief technical observational details; in § 3, we describe and analyze the data (§ 3.1 deals with the optical data, whereas § 3.2 focuses on the millimeter-wave data); we conclude in § 4 with a discussion of the structure of He 2-113 in the context of theoretical models.

2. OBSERVATIONS

2.1. *Optical*

A total of six exposures of He 2-113 (2×20, 2×140, 2×400 s) using the Hα filters [F656N ($\langle\lambda\rangle = 656.2$ nm, $\delta\lambda = 2.2$ nm), taken as part of an *HST* SNAPshot imaging program (GO program 8345) and processed via the standard calibration pipeline, were retrieved from *HST* archives. The nebula lies entirely within the field of the Planetary Camera (800×800 pixels; plate scale = 0.″0456 pixel^{-1}) of WFPC2. Each image of an equal exposure pair was shifted with respect to the other during the observations. After applying a geometric distortion correction, the images were registered to subpixel accuracy (using cross-correlation techniques), followed by cosmic ray removal and correction of saturated pixels in the long exposure images.

2.2. *Millimeter-wave*

Millimeter-wave CO observations of He 2-113 were made using the 15 m SEST (Swedish-ESO Submillimeter Telescope[6]), situated on La Silla, Chile. The CO $J = 1$–0 data were obtained during 1989 August and 1996 May, and the $J = 2$–1 data were obtained during 1990 April and 1991 February, using SIS receivers at 3 and 1.3 mm. The beamwidths of the telescope at the CO $J = 1$–0 and 2–1 frequencies (115 and 230 GHz) are 45″ and 24″, respectively. Acousto-optical spectrometers (AOS) with bandwidths of 1 and 0.5 GHz were used to record the 1–0 and 2–1 spectra. The channel separation was 0.7 MHz, and the resolution was 1.4 MHz. All intensities are given in $T_{\rm mb}$, which is the chopper wheel corrected antenna temperature, T_A^*, divided by the main beam efficiency (0.7 for 1–0 and 0.6 for 2–1). Pointing was checked on nearby SiO maser sources and was generally estimated to be accurate to better than 3″ rms. The telescope was used in a dual beam switch mode with the source alternately placed in each of the two beams, a method that yielded flat baselines and a reliable continuum level. The beam separation was about 11.′5.

3. RESULTS

3.1. *Optical Morphology*

The nebula has an overall bipolar shape, roughly aligned NW–SE (P.A. = 136°) (Fig. 1*a*). The same image with sharp structures enhanced is shown in false color in Figure 1*b*. The SE lobe has a maximum radial extent of about 2.″3, whereas the NW lobe extends to about 1.″9. Both lobes have roughly the same width of about 2.″3. The lobes have fairly sharp edges in the logarithmically stretched image shown in Figure 1*a*, making the above measurements of their dimensions relatively unambiguous. The visible central star lies in the interior of a bright, almost complete elliptical ring (Ring 1) but is clearly offset along P.A. = $-77°$ from the center of this ring, by 0.″18 (270 AU) (Fig. 1*c*). The major axis of Ring 1 is about 1.″3 (1950 AU) in extent, and the minor-to-major axis ratio is about 0.5 (Fig. 1*c*). Roughly two-thirds of a second, fainter, coaxial ringlike structure (Ring 2) can be seen separated from Ring 1 by a dark lane of width 0.″2 (300 AU). The central star is offset from the center of Ring 2 by 0.″31, along P.A. = 71°. The projection of the common axis of these rings on the sky-plane (i.e., line passing through the center of Ring 1 and perpendicular to its major axis) is oriented at a P.A. of $\approx 65°$, neither aligned with, nor perpendicular to, the long axis of the nebula at P.A. = 136°. The rings have a rather knotty appearance. Two additional bright knots can be seen offset to the W and NW of Ring 2 (the NW-knot joins onto the ring structure). Another lobe (hereafter NE-lobe) is seen to extend along P.A. = 55°. It is difficult to discern the counterpart to this lobe on the other side of the star, although a small protrusion can be seen in the SW direction, signifying that if the SW-lobe exists, it must be less extended than the NE one. The rings, especially Ring 1, are by far the brightest structures in the nebula—e.g., the bright regions of Ring 1 are more than 200 times brighter than the NW–SE lobes at their peripheries. The visual appearance of the rings indicates that Ring 2 is located further from us than Ring 1, with its brightness being attenuated by a larger column of nebular dust. From the same reasoning, the NW lobe, whose surface brightness (averaged over a 25° wedge between radial offsets of 0.″7 and 2″ from the central star) is a factor 1.8–2.5 times lower than its SE-counterpart, is the more distant one. Thus, the nebula as a whole is oriented to our line of sight such that Ring 1 and the SE and NE lobes are closer to us than Ring 2 and the NW lobe.

The bright central region of the nebula is surrounded by a faint, roughly round, halo. We can trace the halo out to a radius of at least 10″ using azimuthal averaging to increase the signal-to-noise, as seen in representative radial cuts of the Hα intensity taken from the F656N image (Fig. 2). The halo surface brightness decreases with radius as a $r^{-\beta}$ power-law, where $\beta \approx 2.9 \pm 0.2$, fading smoothly into the noise. It is therefore likely that the actual radius of the halo is significantly larger. The halo brightness is most likely due to scattering by dust of Hα photons emitted from the bright compact central region of the nebula. Although both the scattered light and intrinsic emission from ionized gas should decrease as r^{-3} for an envelope with an inverse-square density profile, the observed halo is unlikely to be due to intrinsic emission because our molecular-line observations directly show the presence of large amounts of neutral matter within $\sim 10''$ of the center (§ 3.2).

We have located the geometrical center of the halo by fitting ellipses to the iso-intensity contours of the halo between offsets of 2.″7 and 3.″5 (Fig. 3), after rebinning the image to pixel sizes 2.5 times larger than those in the original, in order to improve the signal-to-noise (S/N) ratio. The radial range selected is motivated by the dual requirements of getting as far as possible from the asymmetrical central region and still retaining a sufficient signal-to-noise ratio for generating relatively smooth iso-intensity contours. We find that the best-fit ellipses have a minor-to-major axis ratio of 0.96 (i.e., they are nearly circular), and the position angle of the major axis lies roughly along the major axis of the nebula. The centers of these ellipses are offset from the central star by small but significant distances, which are apparently larger for contours with larger radii. Thus, e.g.,

[6] The SEST is operated jointly by ESO and the Swedish National Facility for Radio Astronomy, Onsala Space Observatory, at Chalmers University of Technology.

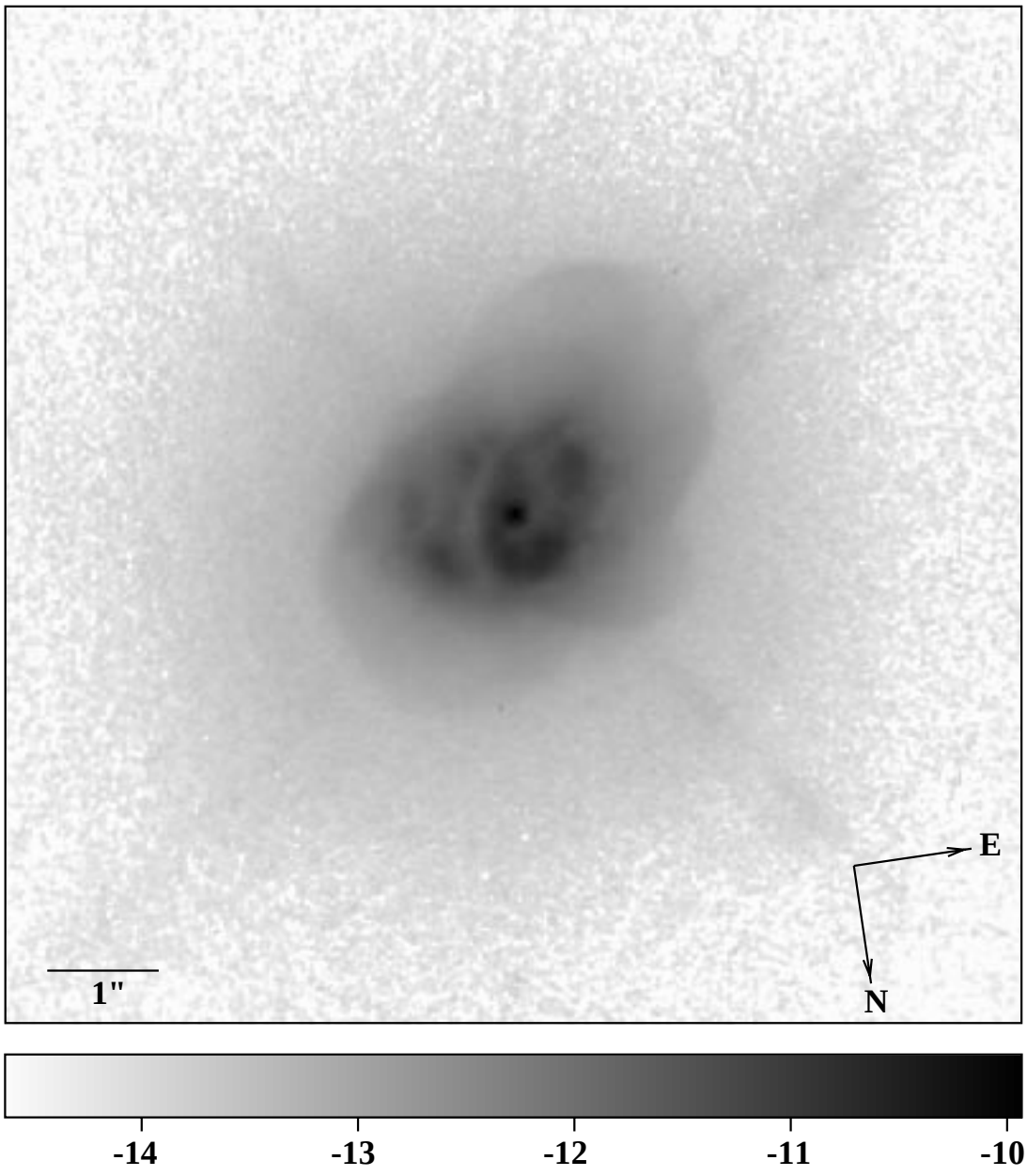

FIG. 1*a*

FIG. 1.—(*a*) Hα (F656N) image of the young planetary nebula He 2-113 taken with the Planetary Camera (resolution 0.″0456 pixel^{-1}) of WFPC2/*HST*. A reverse gray-scale and logarithmic stretch have been used, with the maximum and minimum surface brightnesses on the scale bar shown being 1.17×10^{-10} and 2.33×10^{-15} ergs s^{-1} cm^{-2} arcsec^{-2}. The J2000 coordinates of the visible central star, measured from our image, are $\alpha = 14^{h}59^{m}53^{s}.54$, $\delta = -54°18'07''.7$. (*b*) The false-color image shows the data in (*a*) after processing to enhance sharp structures. The processed image, $Im_P = Im_O/(Im_O + 0.04Im_S)$, where Im_O is the original image, and Im_S is obtained by smoothing Im_O. Various nebular morphological features and dimensions (see text) have been labeled. The tips of the pointers with the labels "SE-lobe" and "NW-lobe" situated closer to the nebular center mark the locations used for determining the radial extents of these lobes.Author original of (*b*) has different color resolution and is available on-line. (*c*) Enlarged view of the central regions of the image shown in (*a*). The dashed curves indicate the features described as Ring 1 and Ring 2 in the text. The maximum and minimum surface brightnesses on the scale bar shown are 9.23×10^{-10} and 5.86×10^{-14} ergs s^{-1} cm^{-2} arcsec^{-2}.

the center of the iso-intensity contour at an average radius of 2.″85 is offset by $\delta x = -0.''094$, $\delta y = -0.''036$ (where the x and y axes are the horizontal and vertical axes in the images in Fig. 1), and the center of the contour at an average radius of 3.″28 is offset by $\delta x = -0.''124$, $\delta y = -0.''036$, from the central star. This result is potentially very important because it would provide strong evidence for relative motion between the central star and the center of symmetry of the ejected material, e.g., due to orbital motion around a widely separated unseen companion. Nevertheless, noting that (i) there are intrinsic departures from smoothness and circularity in the iso-intensity contours, and (ii) these contours do not necessarily represent iso-*density* contours because the halo is at least partly illuminated by a nonsymmetric central source, the above offsets may not be physically significant. However, our measurements of such offsets highlights a hitherto unexplored potential use of high-quality *HST* images—namely, the detection and measurement of offsets of central stars of PNe/PPNe from the centers of the envelopes ejected during AGB evolution.

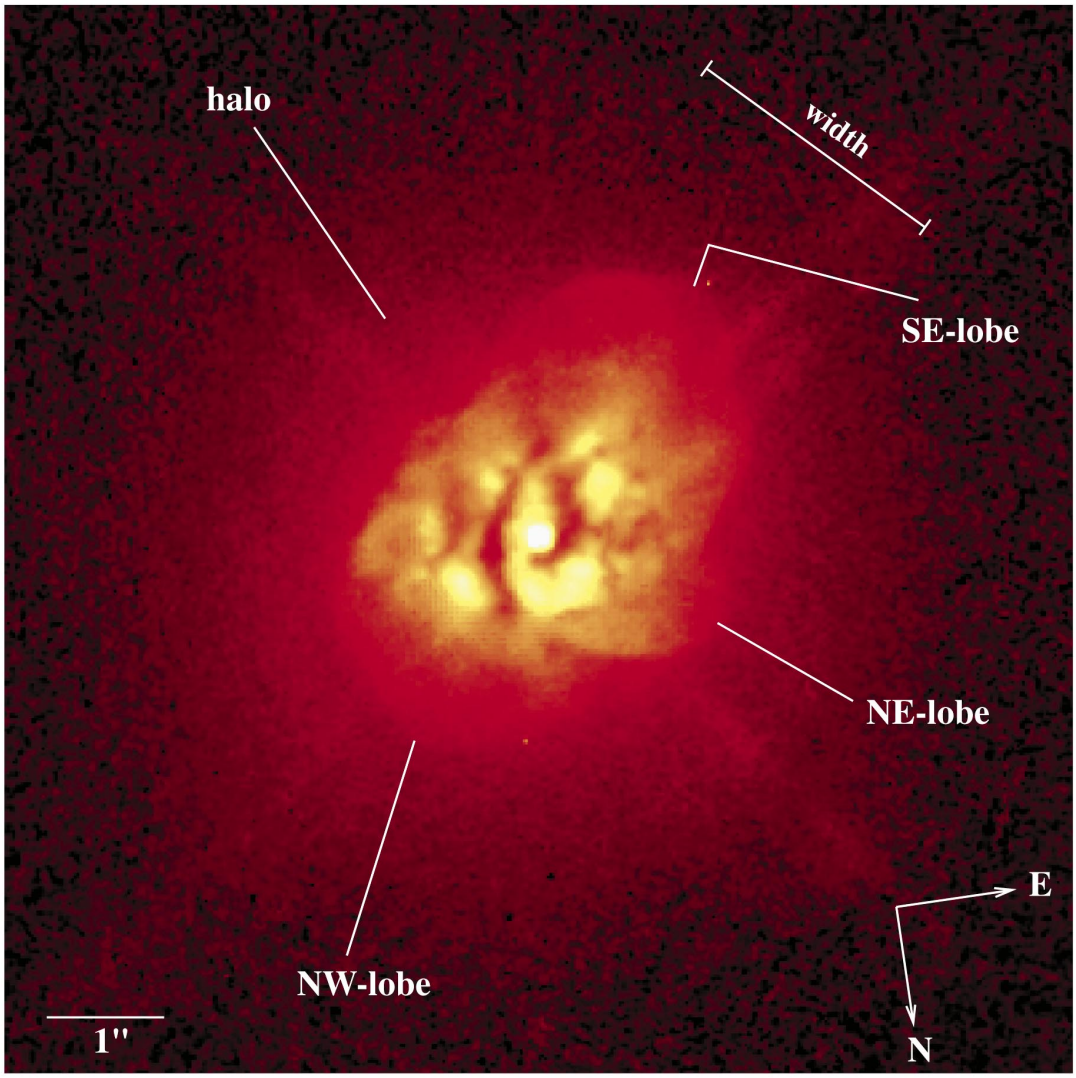

FIG. 1*b*

We note that the morphology of He 2-113 observed in our image bears little resemblance to the Hβ morphology recovered by DBS97 from deconvolving WFPC1 data. This may result from any one or a combination of the following factors: (i) the Hβ morphology is intrinsically different from that of Hα due to variable and higher nebular extinction at the shorter wavelength, (ii) the deconvolved Hβ image artifacts because of DBS97's lack of a good point spread function, and (iii) there is an orientation error in the Hβ image.

The *observed* nebular (i.e., excluding the central star) count rate in our F656N image corresponds to an Hα flux of 1.6×10^{-11} ergs s^{-1} cm^{-2}, which lies within the range of fluxes measured from the ground—1.1×10^{-11} (Acker et al. 1992) to 1.75×10^{-11} ergs s^{-1} cm^{-2} (DBS97). A low-resolution, 0.56–0.99 μm, spectrum of He 2-113 by le Bertre et al. (1989) also shows the Hα line (blended with [N II] λ6586) to be much stronger than the continuum. Thus, it is unlikely that continuum radiation from the nebula at 656 nm (e.g., due to scattered continuum from the central star) contributes significantly to the count rate in the F656N filter. The observed count rate due to the star in our image is 22% of the expected value derived from a 31,000 K (DBS97) blackbody scaled by the observed bolometric flux of the star (see § 3.2.1) and integrated over the F656N filter bandpass. From this result we infer that the line-of-sight extinction optical depth to the star at 656 nm (presumably due to circumstellar dust), $\tau_{\rm ext}$, is 1.5, which implies an A_V of 2, using the average interstellar extinction curve (Whittet 1992). We estimate an uncertainty of about 0.3 mag in our derived A_V due to uncertainties in the *HST* photometry, the predicted stellar flux, and the correction due to the wavelength-dependent extinction. A comparison between the expected visual magnitude derived from the scaled blackbody flux ($m_V = 9.4$), and the observed ground-based value (11.7 ± 0.1; DBS97) implies that A_V is 2.3 ± 0.1, consistent with our *HST*-based estimate. DBS97 derive a significantly higher $A_V = 3.1$ from both the Hα-to-Hβ and radio-to-Hβ flux ratios, probably because their value, which represents an average over all the nebula, includes regions with higher extinction than the line of sight to the central star. The low surface brightness lane between Ring 1 and Ring 2 is most likely such a region of relatively high extinction compared to the line of sight toward the star.

We can make rough estimates of the densities in Ring 1 from its excess Hα surface brightness (over the surrounding nebulosity), I(Hα), which lies in the range of about (3–9) $\times 10^{-12}$ ergs s^{-1} cm^{-2} arcsec^{-2}, and taking a thickness comparable to its width (0.″23 = 5×10^{15} cm). Correcting

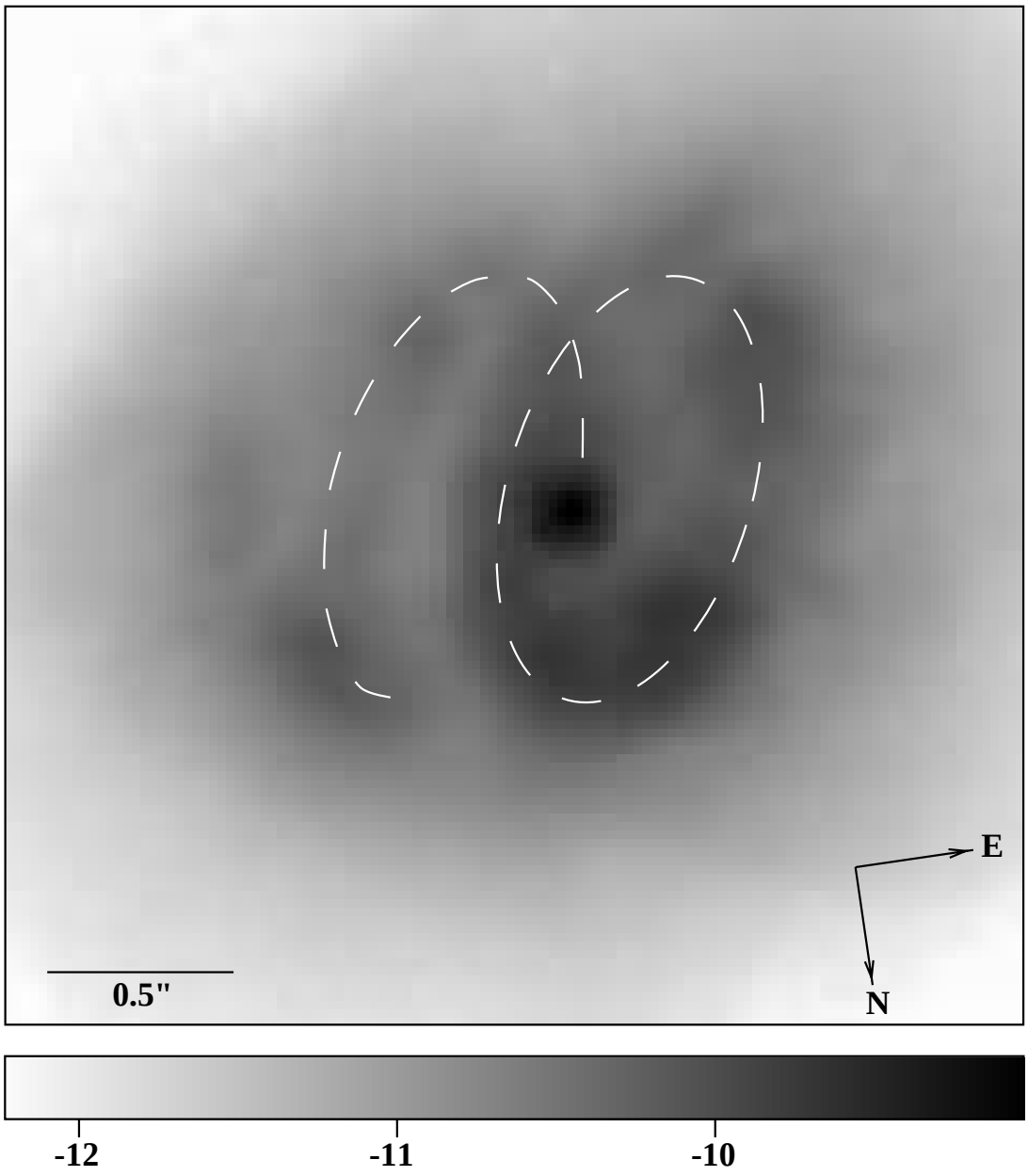

FIG. 1*c*

$I(\mathrm{H}\alpha)$ for the extinction measured toward the star and assuming Case B recombination and an electron temperature of 10^4 K, we find that the density in Ring 1 is roughly about $(0.5\text{–}1) \times 10^5$ cm^{-3}. This density compares well with the average value for the nebula derived by DBS97 (6×10^4 cm^{-3}) from various optical line ratios.

3.2. *Molecular-line Spectra*

The CO spectra are shown in Figure 4. These include the $J = 2\text{–}1$ line (*a*) on-source, and (*b*) average of spectra at positions offset by half a beamwidth from the source center, and (*c*) the on-source 1–0 line. Although the spectrum is relatively noisy, the $J = 2\text{–}1$ on-source line is clearly asymmetric, with a main component extending from approximately -25 to -80 km s^{-1}, with a weak blue wing extending to about -90 km s^{-1} $V_{\rm LSR}$. The broad profile of the main component is typical of emission from the expanding circumstellar envelopes of AGB stars. We use this profile to determine a systemic velocity of -52 km s^{-1} $V_{\rm LSR}$ and an expansion velocity of 28 km s^{-1} for the molecular envelope, using an empirical line-shape fitting procedure as described by Wannier et al. (1990). Our systemic velocity is consistent with that (-58 ± 3 km s^{-1} $V_{\rm LSR}$) derived by DBS97 from the Hα and Hβ nebular emission. Our value of the expansion velocity is consistent with the value (27 km s^{-1}) inferred from the -85 km s^{-1} $V_{\rm LSR}$ absorption feature of the Na-D (λ5889.9) line by DBS97, and somewhat larger than that (19 ± 3 km s^{-1}) inferred by the same authors from the mean full width at half-maximum (FWHM) of the Hα and Hβ lines. This may be because either the FWHM of the Balmer lines underestimates the expansion velocity, or because the neutral material is expanding at a faster rate than the ionized one. The blue wing of the CO $J = 2\text{–}1$ line indicates that part of the molecular envelope material has been accelerated to velocities significantly larger than

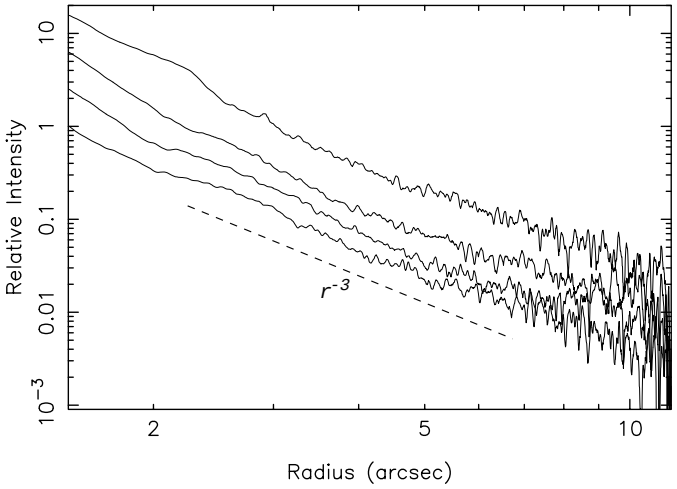

FIG. 2.—Representative azimuthal averages of the radial relative intensity distribution from the Hα image, showing the extended halo. The four curves show azimuthal averages from each of the four quadrants bounded by the diffraction spikes due to the central star. The curves have been displaced vertically by arbitrary amounts for clarity. An r^{-3} power law, e.g., expected for scattering from an envelope with an inverse-square density distribution illuminated by a central source, is also shown for comparison.

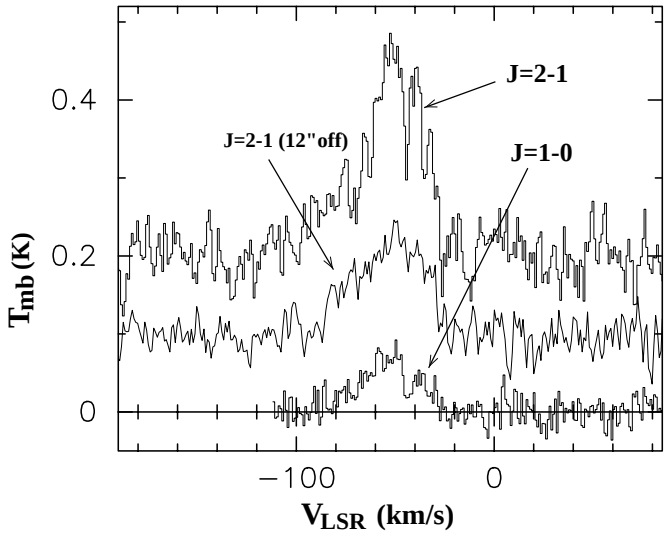

FIG. 4.—CO $J = 1$–0 and 2–1 spectra of He 2-113, taken with the SEST. The spectrum labeled "12″ off" was obtained by averaging 2–1 spectra from four positions offset by half a beamwidth from the source-center along the R.A. and decl. axes; the ratio of the off- to on-source intensity shows that the emission source is unresolved.

28 km s^{-1}; similar evidence for high-velocity neutral material is found by DBS97 from the presence of an Na I absorption component blueshifted by 38 km s^{-1} from the systemic velocity.

The measured fluxes of the main component in the 2–1 and 1–0 lines are 8.4 and 2.4 K km s^{-1}, with about ±15% uncertainty. Our CO $J = 2$–1 line flux is about a factor 1.25 smaller than expected from scaling up the value (7.1 K km s^{-1}) obtained with the CSO 10.4 m telescope (Huggins et al. 1996) for the larger (15 m diameter) SEST aperture. Although pointing errors can result in reduced fluxes for compact sources like He 2-113, we believe the SEST measurement is more accurate because (i) we measured the same value on several different occasions, and (ii) the CSO observations of He 2-113 are limited to very low elevations and therefore high telluric attenuation, necessitating a large and probably uncertain correction. Our five-point map in the $J = 2$–1 line at half-beamwidth spacing (12″) shows that the source is *unresolved*, since the "off" spectrum in Figure 4 is roughly half as intense as the on-source spectrum. Therefore, the emission source has a radius which is $\lesssim 10''$ and larger than the bright central region seen in Hα, i.e., larger than 1″. We can therefore identify the extended halo seen in our Hα image with the inner regions of the molecular envelope seen in CO emission.

In the following sections, we use the CO-line and far-infrared fluxes to estimate the amount of molecular gas and dust in He 2-113.

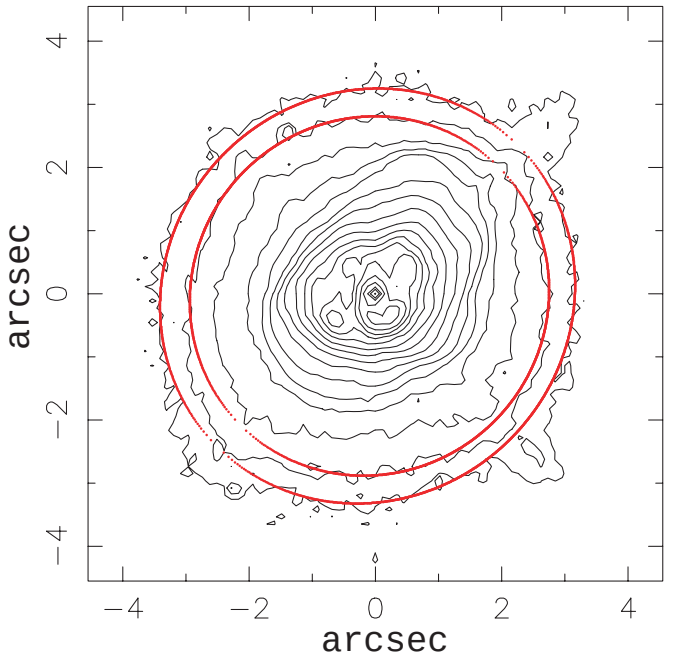

FIG. 3.—Contour plot of the image in Fig. 1*a*, after rebinning to a pixel-size 2.5 times larger than in the original, in order to improve the signal-to-noise ratio. Contours are spaced apart by a multiplicative factor of 1.703, and the surface brightness at the lowest contour is 8.76×10^{-15} ergs s^{-1} cm^{-2} $arcsec^{-2}$. The best-fit ellipses to the two lowest iso-intensity contours are also shown. The centers of these ellipses are offset from the central star (located at 0, 0) by small but significant distances.

3.2.1. *Dust in the Nebula*

Both *IRAS* broadband photometric measurements, *IRAS*-LRS spectra, and more recently, the ISO-SWS spectrum of He 2-113 from 2.4 to 45 μm (Waters et al. 1998) clearly show the presence of a substantial cool dusty envelope around the central star. The ISO spectrum shows a large number of relatively weak features on top of a strong underlying continuum: the continuum is interpreted as arising from amorphous grains, and the discrete features are interpreted as arising due to "carbon-rich" grains (PAHs) and "oxygen-rich" grains (crystalline silicates). We have estimated the dust mass by fitting the far-infrared (from *IRAS*) and *L*- and *K*-band fluxes of He 2-113, using a multi-component dust emission model (Sahai et al. 1991). The *IRAS* photometric fluxes are used in preference to those from the ISO-SWS spectrum because the latter have larger uncertainties (e.g., Cohen et al. 1999). The color-corrected

IRAS fluxes are 111.3, 297.7, 150.6, and 66.6 Jy at 12, 25, 60, and 100 μm, respectively, and the *L*- and *K*-band fluxes are 5.7 and 0.65 Jy (Acker et al. 1992).[7] The presence of strong "PAH" features at 6–9 and 11–13 μm probably results in the *IRAS* 12 μm band flux exceeding that due to the smooth underlying "continuum" by about 10%–20%. A dust emissivity of 150 cm^2 g^{-1} at 60 μm (Jura 1986), with a λ^{-p} power-law variation and $p = 1$ and 1.5 (characteristic of amorphous grains) has been assumed.

We find that a good fit to all the fluxes requires at least three different temperature dust components. The masses and temperatures of the two primary components are as follows: "cold" component—$6.7(5.7) \times 10^{-4}$ $M_\odot$ and 100(106) K for $p = 1.5(1.0)$, and "warm" component—$1.1(1.4) \times 10^{-6}$ $M_\odot$ and 324(378) K for $p = 1.5(1.0)$. Although most of the dust mass lies in the cold component, the warm component is energetically important, since roughly half of the total luminosity is emitted by this component. The mass and temperature of the "hot" component is relatively much more uncertain, lying in the range $(1.5–0.45) \times 10^{-9}$ $M_\odot$ and (670–900) K for $p = 1.5$–1.0. The bolometric flux, obtained by computing the total energy emitted by the model dust components (and not significantly different from that obtained by directly integrating the observed spectral energy distribution) is 7.6×10^{-8} ergs s^{-1} cm^{-2}, corresponding to a luminosity of 5350 $L_\odot$. (The dust mass and the bolometric luminosity are proportional to the square of the distance). The characteristic radius of the far-infrared dust emitting region, r_d, is unknown. If the dust is heated by direct starlight, then $r_d = [(L_* T_{\rm eff}^p)/(16\pi\sigma)]^{1/2} T_d^{-(2+p/2)}$ (Sopka et al. 1985; Herman, Burger, & Penninx 1986), giving $T_d = 100(106)$ K at $r_d = (6.2–1.2) \times 10^{17}$ cm for $T_{\rm eff} = 31{,}000$ K and $p = 1.5(1.0)$. However, because significant reddening of the stellar radiation must occur in the inner regions of the nebula which are optically thick to ultraviolet and visible photons, r_d is likely to be somewhat smaller. Our detailed spherically symmetric model for deriving the gas and dust mass-loss rates (described in the next section) shows that the mass of the "cool" component determined above is contained within a radius of 1.2×10^{17} cm.

De Marco & Crowther (1998) fit the near- and far-IR fluxes of He 2-113 with two blackbody components at temperatures of $\approx$775 and 200 K; however, since the optical depths in the far-IR are quite low [e.g., the (100–12) μm optical depths are 0.007–0.16 in our $p = 1.5$ model, assuming an emitting size of 6″], blackbody fits are invalid. Unfortunately, blackbody fits have been used by many authors in interpreting the far-infrared dust emission spectra of planetary nebulae and related objects, leading to overestimates of the temperature of the dust grains (and consequently, underestimates of their distance from the central star).

3.2.2. *Molecular Gas in the Nebula*

Simple estimates of the molecular mass in planetary nebulae from CO lines have often been made by assuming (a) the emission to be optically thin, and (b) fixed values of the kinetic temperature (typically 10–20 K) (e.g., Huggins et al. 1996) and the [CO]/[H_2] abundance ratio, $f_{\rm CO}$ (typically $\sim 10^{-4}$ in PNe).[8] Such an estimation, assuming a kinetic temperature of 10 K and $f_{\rm CO} \sim 10^{-4}$, yields a total gas mass of 0.9×10^{-2} $M_\odot$ from the 1–0 spectrum, and 1.9×10^{-2} $M_\odot$ from the 2–1 spectrum.

Comparing the gas and dust masses derived above, we find that the gas-to-dust ratio is 25, which is rather low compared to the typical values ($\sim$100–400) found in the circumstellar envelopes of AGB stars. The most likely reason for this discrepancy is that our gas-mass estimate is too low, due to one or both of the following: (i) the actual average kinetic temperature is significantly lower than 10 K, and (ii) the CO emission is optically thick. Much of the outer extended molecular envelope in proto–planetary and young planetary nebulae can be at rather low temperatures, because of an absence of strong heating sources, and cooling due to adiabatic expansion. The most prominent example of this effect is found in the Boomerang Nebula (a PPN), whose CO $J = 1$–0 spectra directly show the presence of ultracold gas with temperatures below that of the microwave background (Sahai & Nyman 1997). Similarly, modeling of the CO spectra of the young PN, M1-16, also shows the presence of gas at quite low temperatures (Sahai et al. 1994).

We have therefore constructed detailed models to fit the He 2-113 CO spectra, using a numerical code which self-consistently accounts for the line excitation, radiative transfer, and line-cooling processes (Sahai 1990) in a spherical envelope expanding with a constant velocity. Dust frictional heating of the gas and cooling due to adiabatic expansion is included. The 60 μm flux is used to constrain the dust density self-consistently. The outer radius of the CO envelope is assumed to be limited by photodissociation by the interstellar ultraviolet (ISUV) radiation field and has been determined using the prescription given by Mamon, Glassgold, & Huggins (1988). We have computed a large number of models with mass-loss rates, $\dot{M}$, in the range $\sim 10^{-5}$ to 2×10^{-4} $M_\odot$ yr^{-1} and find that the $J = 2$–1 and 1–0 data are best fitted with rates near the upper end of the above range—in these models a significant part of the outer envelope is at temperatures below the microwave background temperature. The CO $J = 1$–0 and 2–1 fluxes are found to vary rather nonlinearly with $\dot{M}$, with an increase in $\dot{M}$ leading to a decrease in the observed flux—this is due to the associated decrease in the drift velocity of the grains and therefore in the frictional heating of the gas, leading to a decrease in the kinetic temperature.

The best fit models give $\dot{M} \sim (0.9 \pm 0.2) \times 10^{-4}$ $M_\odot$ yr^{-1} characterizing the AGB CSE in He 2-113, assuming $f_{\rm CO} = 10^{-4}$. The corresponding model intensities ($T_{\rm mb}$) and integrated line fluxes are 0.057 K and 2.3 K km s^{-1} for the $J = 1$–0 line and 0.23 K and 9.6 K km s^{-1} for the $J = 2$–1 line, which compare well with the observed values. The mass-loss rate would be (i) higher for a larger distance to He

[7] independent IR photometry by le Bertre et al. (1989) and Webster & Glass (1974) is consistent with these fluxes.

[8] The [CO]/[H_2] ratio in carbon-rich (C/O > 1) AGB outflows is believed to be determined by the O/H abundance, and for full association of O into CO, would be 9.6×10^{-4} in He 2-113, which has O/H = 4.8×10^{-4} (DBS97). However, in objects like He 2-113, which contain a significant flux of ultraviolet radiation from the central star, the actual CO abundance is expected to be significantly lower due to photodissociation. Modeling of observations of circumstellar CO in the supergiant α Ori and the young PN, NGC 7027, both of which have significant UV fluxes, indicate that $f_{\rm CO} \sim 5 \times 10^{-5}$–$10^{-4}$ (Huggins 1987; Deguchi et al. 1990).

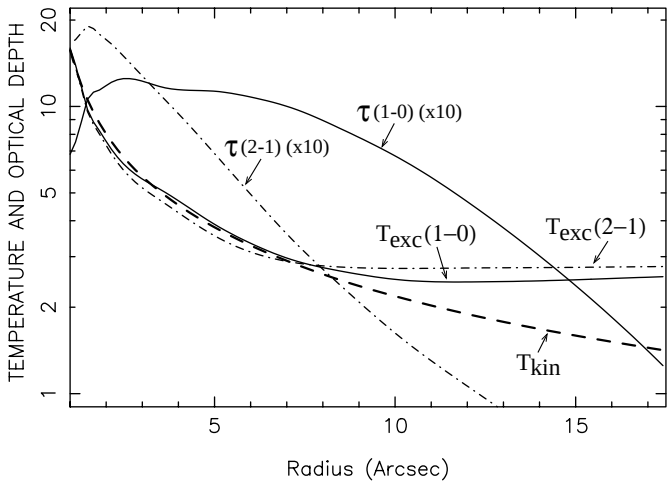

FIG. 5.—The excitation temperatures and tangential optical depths of the CO $J = 1$–0 and 2–1 lines, as well as the kinetic temperature for the best-fit model of the millimeter-wave CO line emission from He 2-113. The optical depths have been scaled up by a factor of 10.

2-113, but the actual dependency cannot be simply predicted (e.g., Sahai 1990), and (ii) lower for a higher value of f_{CO}, but the percentage decrease in $\dot{M}$ could be smaller than the percentage increase in f_{CO} because the increased CO abundance would lead to increased cooling and therefore lower kinetic temperatures. Both $p = 1$ and 1.5 models were constructed; the larger value of p provided better fits. The gas-to-dust (mass) density ratio in these models is about 190. The excitation temperatures and tangential optical depths of the CO $J = 1$–0 and 2–1 lines, as well as the kinetic temperature for this model are shown in Figure 5. The gas is quite cold in most regions of the envelope, with temperatures below 5 K for radii $\gtrsim 3''.7$, falling below the microwave background temperature (2.8 K) beyond a radius of about 7″. Note that in contrast to the Boomerang Nebula, no observable *negative intensity* wings are found in the 1–0 line profile of He 2-113. This is because the AGB mass-loss rate in He 2-113 is not high enough to result in a $J = 1$–0 optical depth significantly larger than unity in the region where the kinetic temperature falls below 2.8 K. The CO data allow us to set only a lower limit on the total mass, M_{env}, of the AGB circumstellar envelope, because (a) the *total* extent of the envelope is unknown and M_{env} increases linearly with radius, and (b) the observed CO line fluxes are brightness limited. We find that $M_{env} = 0.32(R_{out}/3 \times 10^{17}$ cm) $M_\odot$, where R_{out} is the actual outer radius of the envelope (and 3×10^{17}cm is the radius at which the CO abundance falls to half its initial value due to photodissociation by the ISUV flux). We conclude this section with a strong cautionary note: without a detailed investigation of the excitation conditions and optical depths of the CO $J = 1$–0 and 2–1 millimeter-wave lines, simple molecular mass estimations in planetary nebulae can easily lead to large underestimates because *the* CO *lines can be subthermally excited and optically thick.*

4. THE STRUCTURE OF He 2-113

Our imaging of He 2-113 reveals the geometry of the mass-loss process both during the AGB and the post-AGB evolutionary phases. The round halo region is most likely the remnant of the circumstellar envelope produced during the spherical mass-loss phase when the central star was an AGB red giant. The aspherical central regions are characteristic of the strong departures from circular symmetry which are observed to occur as AGB stars transition into the post-AGB evolutionary phase. Waters et al. (1998) conclude that the presence of features from "hot" C-rich dust and "cool" O-rich dust in objects like He 2-113 and BD +30°3639 is better explained by a thermal pulse occurring early in the post-AGB evolution, rather than much later, when the central star is on the WD cooling track. Assuming a lower limit of 28 km s^{-1} for the expansion velocity of these lobes, we estimate that the expansion age of the main lobes is $\lesssim 550$ yr.

The very aspherical nature of the nebula surrounding the central star in He 2-113 may help, at least partially, in explaining the large ratio (35) found by De Marco & Crowther (1998) between the number of ionizing photons predicted by their modeling and the number derived from the nebular Hβ flux using the Zanstra assumption that the nebula is optically thick to ionizing photons. Although some significant fraction of the ionizing continuum may be absorbed by dust and not by gas (De Marco & Crowther 1998; Aitken et al. 1980), our imaging shows that ionizing radiation may also be escaping preferentially from the nebula along directions with relatively low optical depth. Such directions could lie along the main bipolar axis, and/or the axis of the NE lobe.

How can we explain the formation of the complex nebular structure seen in He 2-113? Until recently, the generalized interacting stellar winds ("GISW") model was considered to be very successful in explaining the morphology and formation of aspherical PNe (Balick 1987). In this model, various *axisymmetric*, *bipolar* PN shapes are obtained by the interaction of a very fast central-star wind with the progenitor AGB CSE (Kwok 1982), when the latter is denser near the equator than the poles (Balick 1987). The discovery that *multipolar and point-symmetric* structures are ubiquitous in young planetary nebulae (ST98; Sahai 2000) indicates that the GISW model needs to be modified significantly. ST98 suggest that fast, collimated outflows which can change their direction with time, are the primary agents for shaping PNe. The observed structure of He 2-113, with its main pair of bipolar lobes, two rings, and a third lobe (i.e., the NE-lobe), all with different geometric axes, is not consistent with the GISW model. The multipolar structure supports the ST98 model of PN formation. Direct evidence for a fast outflow in He 2-113 comes from spectroscopic observations of De Marco & Crowther (1998) and Leuenhagen, Hamann, & Jeffrey (1996), who find that the central star is currently losing mass in a wind with an outflow velocity of 160–200 km s^{-1} and at a rate of 0.8×10^{-6} $M_\odot$ yr^{-1}. The blue wing seen in our CO $J = 2$–1 profile indicates that some part of the molecular envelope has been accelerated to high velocities by this outflow. The presence of shocked gas resulting from the interaction of the fast outflow with the molecular envelope, comes from the detection of relatively bright emission in the $v = 1$–0 $S(1)$ 2.121 μm line of H_2 and the 1.785 and 2.223 μm lines of [Fe II] by le Bertre et al. (1989).

He 2-113 is not unique in showing multiple geometrical structures. Most young planetary nebulae, when imaged with *HST*'s resolution, show such structures (e.g., ST98; Sahai et al. 1999d). Two other PNe with WC central stars, M4-18 and BD +30°3639, have been imaged with WFPC2

in Hα. M4-18 shows the presence of a main inclined equatorial toroid, and an additional pair of fainter elliptical limb-brightened structures with their major axes at about $\pm 45°$ relative to the toroidal axis in the sky plane (ST98). BD $+30°3639$ shows a main ring structure, best interpreted as a squat cylindrical shell with its axis inclined at a modest angle to the line of sight; multiple radial streaks and a faint detached nebulous clump indicate the ejection of matter in fast collimated outflows (ST98). Although PNe showing a single bright ring may be simply explained in the GISW model as representing the dense waist of a bipolar nebula seen nearly pole-on, clearly this explanation does not work when more than one ring is present, or when the ring is not coaxial with the bipolar axis (as in He 2-113). Binary models, in which a low-mass companion spirals into the extended atmosphere of the mass-losing primary star, producing an enhanced mass-loss episode or the ejection of a common envelope which is confined to a preferred plane (Morris 1981; Livio 1993), also fail in this case. Ring 1 and Ring 2 in He 2-113 could be the enhanced-brightness rims of a small *inner* tilted hourglass structure—such structures have now been found in three PNe [MyCn 18 (Sahai et al. 1999d), He 2-104 (ST98), and Hubble 12 (Welch et al. 1999)]. At present, there is no satisfactory model for creating the ringlike structures seen in He 2-113 or other PNe (irrespective of whether or not these form the enhanced-brightness rims of an hourglass).

Finally, the central star is conspicuously offset from the centers of both Ring 1 and 2 and is also not located symmetrically between these centers. It is also offset from the midpoint of the line joining the tips of the main NW-SE lobes of the nebula. Although the latter offset could simply result from the collimated outflow responsible for producing the lobes ploughing into an envelope with slightly dissimilar densities in the NW and SE hemispheres, this explanation is unlikely because the brightness of the halo outside each of these lobes is almost identical, implying a very symmetric progenitor AGB envelope. Thus, He 2-113 joins the Etched Hourglass Nebula (MyCn 18) in having a central star which is offset from the geometrical centers of the different morphological components of the nebula (Sahai et al. 1999d). Sahai et al. (1999d) discuss various mechanisms for producing the offset central star in MyCn 18 and conclude that those involving a binary central star probably offer the best hope of a successful explanation; it is likely that the same conclusion applies to He 2-113 as well. We note that no significant photometric variations on any timescale have been noted in He 2-113, which may impose significant constraints on specific binary models. The geometrical complexity of these nebulae suggests that multiple substellar companions may also play a significant role in their formation.

R. S. thanks an anonymous referee for his/her detailed comments, and NASA for partial financial support for this work from a Long Term Space Astrophysics grant (399-20-61-00-00) and GO grant 08345.01-97A from the Space Telescope Science Institute.

REFERENCES

Aaquist, O. B., & Kwok, S. 1991, ApJ, 378, 599
Acker, A., Ochsenbein, F., Stenholm, B., Tylenda, R., Marcout, J., & Schohn, S. 1992, Strasbourg-ESO Catalog of Galactic Planetary Nebulae (Garching: ESO)
Aitken, D. K., Barlow, M. J., Roche, P. F., & Spenser, P. M. 1980, MNRAS, 192, 679
Balick, B. 1987, AJ, 94, 671
Bowers, P. F., Johnston, K. J., & Spencer, J. H. 1983, ApJ, 274, 733
Cohen, M., Barlow, M. J., Sylvester, R. J., Liu, X.-W, Cox, P., Lim, T., Schmitt, B., & Speck, A. K. 1999, ApJ, 513, L135
Crowther, P. A. De Marco, O., & Barlow, M. J. 1998, MNRAS, 296, 367
Deguchi, S., Izumiura, H., Kaifu, N., Mao, X., Nguyen-Q-Rieu, Ukita, N. 1990, ApJ, 351, 522
De Marco, O., Barlow, M. J., & Storey, P. J. 1997, MNRAS, 292, 86 (DBS97)
De Marco, O., & Crowther, P. A. 1998, MNRAS, 296, 419
Jura, M. 1986, ApJ, 303, 327
Gorny, S. K., & Stasinska, G. 1995, A&A, 303, 893
Herman, J., Burger, J. H., & Penninx, W. H. 1986, A&A, 167, 247
Huggins, P. J. 1987, ApJ, 313, 400
Huggins, P. J., Bachiller, R., Cox, P., & Forveille, T. 1996, A&A, 315, 284
Iben, I. Jr., Kaler, J. B., Truran, J. W., Renzini, A. 1983, ApJ, 264, 605
Kwok, S. 1982, ApJ, 258, 280
Kwok, S., Su, K. Y. L., & Hrivnak, B. 1998, ApJ, 501, L117
le Bertre, T., Epchtein, N., Gouiffes, C., Heydari-Malayeri, M., & Perrier, C. 1989, A&A, 225, 417
Leuenhagen, U., Hamann, W.-R., & Jeffrey, C. S. 1996, A&A, 312, 167
Livio, M. 1993, in IAU Symp. 155, Planetary Nebulae, ed. R. Weinberger & A. Acker (Dordrecht: Kluwer), 279
Mamon, G. A., Glassgold, A. E., & Huggins, P. J. 1988, ApJ, 328, 797
Morris, M. 1981, ApJ, 249, 572
Neri, R., Kahane, C., Lucas, R., Bujarrabal, V., & Loup, C. 1998, A&AS, 130, 1
Sahai, R. 1990, ApJ, 362, 652
———. 1999, ApJ, 524, L125
———. 2000, in ASP Conf. Ser. 199, Asymmetrical Planetary Nebulae II: From Origins to Microstructures, ed. J.H. Kastner, N. Soker, & S. Rappaport (San Francisco: ASP), 209
Sahai, R., & Bieging, J. H. 1993, AJ, 105, 595
Sahai, R., Bujarrabal, V., & Zijlstra, A. 1999a, ApJ, 518, L115
Sahai, R., & Nyman, L.-Å. 1997, ApJ, 487, L155
Sahai, R., te Lintel Hekkert, P., Morris, M., Zijlstra, A., Likkel, L. 1999b, ApJ, 514, L115
Sahai, R., & Trauger, J. T. 1998, AJ, 116, 1357 (ST98)
Sahai, R., Wootten, A., Schwarz, H. E., & Clegg, R. E. S. 1991, A&A, 251, 560
Sahai, R., Wootten, A., Schwarz, H. E., & Wild, W. 1994, ApJ, 428, 237
Sahai, R., et al. 1998, ApJ, 493, 301
Sahai, R., Zijlstra, A., Bujarrabal, V., te Lintel Hekkert, P. 1999c, AJ, 117, 1408
Sahai, R., et al. 1999d, AJ, 118, 468
Schwarz, H. E., Corradi, R. J. M., & Melnick, J. 1992, A&AS, 96, 23
Sopka, R. J., Hildebrand, R., Jaffe, D. T., Gatley, I., Roellig, T., Werner, M., Jura, M., & Zuckerman, B. 1985, ApJ, 294, 242
Su, K. Y. L., Volk, K., Kwok, S., Hrivnak, B. J. 1998, ApJ, 508, 744
Wannier, P. G., Sahai, R., Andersson, B.-G., & Johnson, H. R. 1990, ApJ, 358, 251
Waters, L. B. F. M., et al. 1998, A&A, 331, L61
Webster, L. B., & Glass, I. S. 1974, MNRAS, 166, 491
Welch, C. A., Frank, A., Pipher, Judith L., Forrest, W. J., Woodward, Charles E. 1999, ApJ, 522, L69
Whittet, D. C. B. 1992, Dust in the Galactic Environment, (Bristol: Inst. Phys. Publ.), 67